23rd International Conference
ENGINEERING MECHANICS 2017
Svratka, Czech Republic, 15 – 18 May 2017

EFFECTIVE ELASTIC AND STRENGTH PROPERTIES OF UNIDIRECTIONAL FIBROUS CERAMIC COMPOSITES

S. Valentová*, J. Vorel, M. Šejnoha*****

Abstract: *The present paper is concerned with the evaluation of effective properties and macroscopic tensile strengths of unidirectional fibrous composites made of basal fibers bonded to a ceramic matrix. The actual random distribution of fibers in transverse plane is taken into through the application of statistically equivalent periodic unit cell. A simple maximum stress failure criterion, combined with a linear format of traction separation law, is used to track the onset and subsequent gradual evolution of damage in the composite. The resulting macroscopic stress-strain curves are finally examined to define the searched macroscopic strength of the composite needed, e.g. in the meso-scale analysis of plain weave textile composites.*

Keywords: Spruce, Thermal conductivity, Moisture diffusivity, Homogenization, Mori-Tanaka method.

1. Introduction

Owing to a relatively low cost at one hand and good mechanical properties comparable to glass fibers (Černý et al., 2007), the basalt fiber based composites have received considerable attention in recent years. Due to their good thermal stability the basalt fibers can serve as reinforcement of ceramic matrices manufactured by means of heat treatment such as pyrolysis of, e.g. polysiloxane resins (Glogar et al., 2007a, Černý et al., 2009). When referring to this type of composite, a number of studies addressing fracture properties is also available (Glogar et al., 2007b).

Apart from elastic behavior, see e.g. (Vorel et al., 2015), little attention, however, has been accorded to composite system reinforced by textiles. This might be attributed to the complexity of the microstructure at various scales as see in Fig. 1. To reflect a random nature of fiber distribution in individual yarns as well as various imperfection at the level of plies developed during fabrication, the concept of statistically equivalent periodic unit cell (SEPUC) is usually adopted to define a suitable representative volume element at a respective scale (Šejnoha et al., 2013).

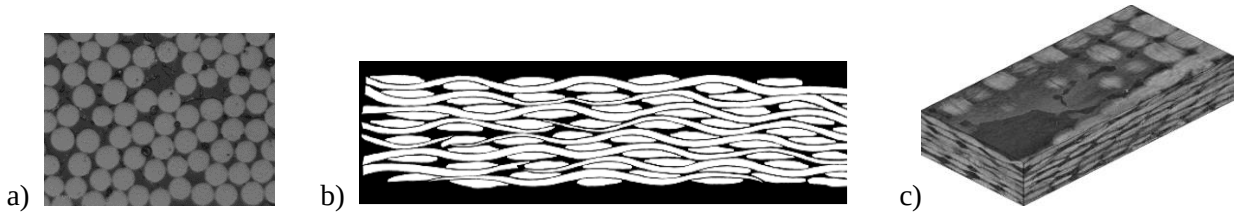

Fig. 1: Micro and meso-structure of basal fiber/ceramic matrix plain weave textile composites: a) level of yarns, b) binary image of the 8-layer laminate cross-section, c) reconstructed CT-scan.

Because of considerable brittleness of the matrix and fibers, the analysis beyond elasticity often draws on the concept of damage mechanics, see e.g. (Šmilauer et al., 2011, Zhou et al., 2013) with particular application to textiles. This approach is also adopted in the present study. Due to space limitation we

* Ing. Soňa Valentová: Czech Technical University in Prague, Thákurova 7; 166 29, Prague; CZ, sona.urbanova@fsv.cvut.cz
** Assoc. Prof. Ing. Jan Vorel, PhD.: Czech Technical University in Prague, Thákurova 7; 166 29, Prague; jan.vorel@fsv.cvut.cz
*** Prof. Ing. Michal Šejnoha, PhD., DSc.: Czech Technical University in Prague, Thákurova 7; 166 29, Prague; CZ, sejnom@fsv.cvut.cz

address the level of yarns only by examining the nonlinear response of the unidirectional fibrous composite, see Fig. 1a.

2. Theoretical formulation

The influence of random distribution fibers in the cross-sectional plane on the macroscopic response is investigated by considering two different SEPUC plotted in Fig. 2. Their construction is described in detail in (Šejnoha et al., 2013).

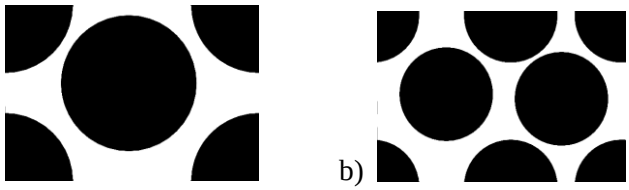

Fig. 2: Examples of SEPUC at the level of yarns: a) two-fiber SEPUC-1, b) five-fiber SEPUC-2.

The elastic material properties partially taken from (Černý et al., 2009) and partially derived from nanoindentation are listed in Tab. 1.

Tab. 1: Material parameters of individual phases.

Material	E **[GPa]**	G **[GPa]**	υ **[-]**	G_f **[N/mm]**	S_T **[GPa]**
Fiber - longitudinal direction	100	25	0.24	-	2.0
Fiber – transverse direction	18	6.4	0.4	-	0.5
Matrix	80	32.3	0.24	0.001	0.08

2.1. Evaluation of effective properties

To verify the computational implementation we begin by deriving the effective elastic properties using both the 1st order homogenization approach and the Mori-Tanaka method (Vorel et al., 2015), where the latter one is also discussed in details in (Šejnoha et al., 2013). In the framework of 1st order homogenization we begin by writing the local displacements and local strains in terms of macroscopically constant strain $\boldsymbol{E}$ and fluctuation displacement $u^*$and strain ε^* fields, which are periodic, as

$$u_i(x) = E_{ij}x_j + u_i^*(x), \quad \varepsilon(x) = \boldsymbol{E} + \varepsilon^*(x). \tag{1}$$

Applying the Hill's lemma yields the system of equations to be solved for unknown displacements and macroscopic strains

$$\delta \boldsymbol{E}^T \boldsymbol{\Sigma} = \delta \boldsymbol{E}^T (\langle \boldsymbol{L}(x) \rangle \boldsymbol{E} + \langle \boldsymbol{L}(x) \varepsilon^*(x) \rangle), \tag{2}$$
$$0 = \langle \delta \varepsilon^{*T}(x) \boldsymbol{L}(x) \rangle \boldsymbol{E} + \langle \delta \varepsilon^{*T}(x) \boldsymbol{L}(x) \varepsilon^*(x) \rangle,$$

where $\boldsymbol{\Sigma}$ represents the prescribed macroscopic stress. Note that under strain loading (E is prescribed) conditions the first equation disappears since $\delta \boldsymbol{E}^T = 0$. Solving Eq. (2) for six unit load vectors then yields the macroscopic compliance matrix. The extracted effective moduli, together with the Mori-Tanaka results, are listed in Tab. 1. Evidently, in case of elasticity, the response provided by the two SEPUC agrees well with the Mori-Tanaka predictions.

Tab. 2: Effective elastic moduli.

	E_{11} **[GPa]**	E_{22} **[GPa]**	E_{33} **[GPa]**	G_{23} **[GPa]**	G_{31} **[GPa]**	G_{12} **[GPa]**	c_f **[-]**
SEPUC-1 – FEM	30.9	29.8	92.4	27.5	27.6	12.4	0.62
SEPUC-2 – FEM	29.9	30.7	92.4	27.6	27.5	12.6	0.62
Mori-Tanaka method	32.6	32.6	92.4	27.6	27.6	12.1	0.62

2.2. Progressive damage formulation

The present analysis builds upon classical continuum damage mechanics with the crack band model to yield objective results. To proceed with the formulation, we begin by writing the constitutive equation for 1D model in the form

$$\varepsilon = \frac{\sigma}{E} + \varepsilon_c, \quad \varepsilon_c = \frac{w_c}{L_s} = (1-D)E\varepsilon, \tag{3}$$

where ε_c, w_c are the crack strain and the crack opening displacement, respectively, $L_s = \sqrt[3]{V_e}$ represents the size of the band to which the cracks are localized (here related to the finite element volume V_e), and D is the damage parameter to reflect a material degradation with the evolution of cracks. In the context of damage mechanics, this is associated with a suitable traction-separation law, which is assumed linear in the present analysis, see Fig. 3.

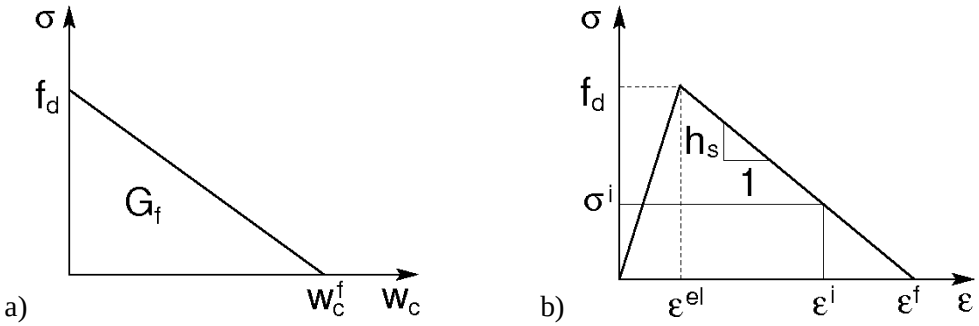

Fig. 3: Linear softening law: a) stress-crack opening displacement diagram, b) stress-strain diagram with linear softening.

The principal material parameter, entering the nonlinear constitutive model, is the fracture energy G_f [N/mm], which corresponds to the area under the stress-crack displacement opening diagram in Fig. 3a

$$G_f = \int_0^{w_c^f} \sigma \mathrm{d}w_c = L_s \int_0^{f_d} (\varepsilon - \varepsilon^{el}) \mathrm{d}\sigma = L_s \int_0^{\varepsilon^f} \sigma \mathrm{d}\varepsilon. \tag{4}$$

It follows from Eq. (4) and Fig. 3(b) that

$$G_f = L_s \left(\frac{1}{2} f_d \varepsilon^f\right) > G_f^{min} = \frac{f_d^2 L_s}{2E}, \tag{5}$$

$$\varepsilon^f = \frac{2G_f}{L_s f_d}, \quad w_c^f = \varepsilon^f L_s = \frac{2G_f}{f_d}. \tag{6}$$

Clearly, while the fracture energy is a material property independent of mesh, the failure strain depends on the smearing distance and thus the mesh characteristics. A simple maximum stress criterion is adopted in the present study

$$F_{1T} = \left(\frac{\sigma_{11}}{S_{1T}}\right)^2, \quad F_{2T} = \left(\frac{\sigma_{22}}{S_{2T}}\right)^2, \quad F_{3T} = \left(\frac{\sigma_{33}}{S_{3T}}\right)^2. \tag{7}$$

where $S_{JT}$is the tensile strength in the direction J. Assuming linear softening the damage parameter D evolves as

$$D_J = \frac{\varepsilon_{eq}^{Ji}(\varepsilon_{eq}^{Jf} - \varepsilon_{eq}^{J})}{\varepsilon_{eq}^{J}(\varepsilon_{eq}^{Jf} - \varepsilon_{eq}^{Ji})}, \quad J = 1T, 2T, 3T, \tag{8}$$

where in case of 3D analysis the uniaxial tensile strain ε is replaced by an equivalent strain $\varepsilon_{eq} = \sqrt{\varepsilon_{ii}^2}$. In Eq. (8), ε_{eq}^{Ji} represents the equivalent strain at the onset of failure whereas ε_{eq}^{Jf} is the strain at complete separation, recall Fig. 3b.

3. Numerical experiments

As an example, we consider the two periodic unit cells in Fig. 2 loaded in the transverse direction by the prescribed increments of the macroscopic tensile stress $\Sigma_{JJ} = \Sigma_{11}$ (J=3 is the fiber direction). The necessary material parameters are available in Tab. 2. The resulting macroscopic stress-strain curves are

plotted in Fig. 4a. The points associated with the assumed tensile macroscopic strength are marked. In cases, where no visible deviation from the linearity is detected, as is the case of SEPUC1, the tensile strength is defined at intersection of the stress-strain diagram with the line of the same elastic stiffness with 5 x 10^{-5} strain offset. The distributions of damage patterns for SEPUC1 associated with the assumed tensile strength and the maximum stress reached are drawn for illustration in Fig. 4b.

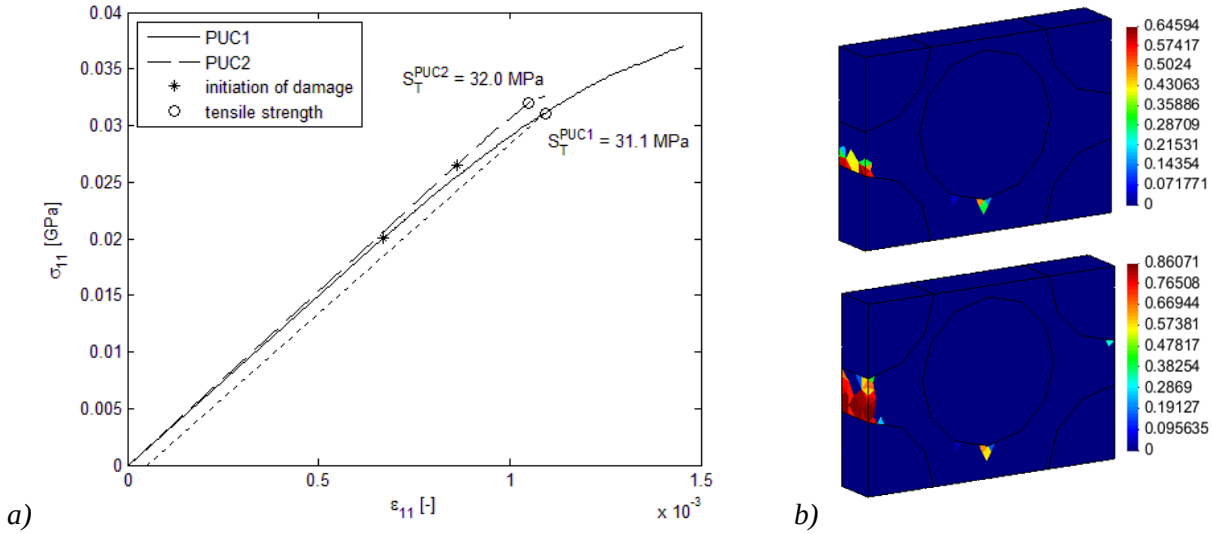

Fig. 4: a) Macroscopic stress-strain curves, b) Damage patterns at $\Sigma_{11} = \Sigma_{1T}$ and $\Sigma_{11} = \Sigma_{11}^{max}$.

4. Conclusions

The presented contribution was concerned with the derivation of effective elastic properties and macroscopic tensile strength of unidirectional basalt fiber reinforced ceramic matrix composite through virtual numerical experiment. These parameters will be subsequently used in an independent meso-scale analysis of the textile laminate where yarns will be considered as homogeneous. Such an analysis will also call for the effective yarn fracture energy. This quantity can be derived from similar experiments but under strain control conditions to allow for softening evolution on macroscale. This study will be presented elsewhere.

Acknowledgement

The financial support provided by the SGS project with the application registered under the No. OHK1-014/17 is gratefully acknowledged.

References

Černý, M., Glogar, P., Giliáš, V., Hruška, J., Jakeš, P., Sucharda, Z. and Vávrová, I. (2007) Comparison of mechanical properties and structural changes of continuous basalt and glass fibres at elevated temperatures, Ceramics − Silikáty, 51(2), pp. 82-88.

Černý, M., Glogar, P. and Sucharda, Z. (2009) Mechanical Properties of Basalt Fiber Reinforced Composites Prepared by Partial Pyrolysis of a Polymer Precursor. Journal of Composite Materials, 43(9), pp. 1109-1120.

Glogar, P., Sucharda, Z., Černý, M., Puchegger, S. and Peterlik, H. (2007a) Microstructure and mechanical properties of heat resistant composites reinforced with basalt fibers. Ceramics − Silikáty, 51(4), pp. 190-197.

Glogar, P., Černý, M. and Tolde, Z. (2007b) Fracture behaviour of the basalt fibre reiforced composites with polysilxane-derived matrix. Acta Geodynamica et Geomaterialia, 4(2), pp. 27-37.

Šejnoha, M. and Zeman, J. (2013) Micromechanics in practice, WIT Press, Boston.

Šmilauer, V., Hoover, Ch.G., Bažant, Z.P., Caner, F.C., Waas, A.M. and Shahwan, K.L. (2011) Multiscale simulation of fracture of braided composites via repetitive unit cells. Engineering Fracture Mechanics, 78, pp. 901-918.

Vorel, J., Grippon, E. and Šejnoha, M. (2015) Effective thermoelastic properties of polysiloxane matrix based plain weave textile composites. International Journal for Multiscale Computational Engineering, 13, 181-200.

Zhou, Y., Lu, X. and Yang, Z. (2013) Progressive damage analysis and strength prediction of 2D plain weave composites. Composites: Part B, 47, pp. 220-229.